Journal of *Marine Science and Engineering*

MDPI

Article

Experimental Study on the Bearing Performance of Rock-Socketed Concrete-Filled Steel Tube Piles under Horizontal Cyclic Loading

Mingwei Liu, Fayou Wu *, Erdi Abi, Linjian Wu *, Yafeng Han, Nirui Chen and Jue Chen

National Engineering Research Center for Inland Waterway Regulation, School of River and Ocean Engineering, Chongqing Jiaotong University, 66 Xuefu Road, Nan'an District, Chongqing 400074, China
* Correspondence: wfyou2020@126.com (F.W.); wljabgf@126.com (L.W.)

Abstract: Rock-socketed concrete-filled steel tube piles (RSCFSTs), which have been widely used in harbors, bridges, and offshore wind turbines, were exposed to horizontal cyclic loading during service and suffered fatigue damage. For the RSCFSTs, longitudinal steel bars were welded to the inner wall of the steel tube to enhance the bonding strength of the steel tube and concrete core interface. It is essential to research the bearing performance of RSCFSTs like this, under horizontal cyclic loading. In this paper, cyclic loading tests of RSCFSTs under horizontal loading were carried out. The failure patterns of RSCFSTs during the destabilization process were generalized, and the lateral displacement development law of RSCFSTs was analyzed. The interfacial bonding characteristics between the steel tube and concrete core during the test were also discussed. Results showed that the horizontal bearing capacity of RSCFSTs decreases nonlinearly with the increase in the equal amplitude of load, and the development process of the lateral displacement-cycle number curve was divided into three phases: (I) rapid growth period, (II) fatigue growth period, and (III) sharp growth period. The larger the horizontal load was, the faster the lateral displacement entered the fatigue growth period. The duration of the rapid growth period and fatigue damage period accounts for about 90% of the total life of RSCFSTs. The stiffening form of the longitudinal steel bars welded to the inner wall of the steel tube can realize the synergistic force between the upper steel tube and the concrete core of RSCFSTs, which accounts for about 7/10 of the length of RSCFSTs. The depth of the steel tube, foundation stiffness, and bonding performance between the steel tube and the concrete core were the key factors that affected the horizontal bearing performance of RSCFSTs. Finally, some constructive suggestions are proposed for the design of RSCFSTs, including increasing steel tube embedded depth, adding a sniffer bar between the steel tube and concrete interface, etc.

Keywords: rock-socketed concrete-filled steel tube piles; horizontal cyclic loading; failure patterns; steel–concrete interface; bonding characteristics

check for updates

Citation: Liu, M.; Wu, F.; Abi, E.; Wu, L.; Han, Y.; Chen, N.; Chen, J. Experimental Study on the Bearing Performance of Rock-Socketed Concrete-Filled Steel Tube Piles under Horizontal Cyclic Loading. *J. Mar. Sci. Eng.* **2023**, *11*, 788. https://doi.org/10.3390/jmse11040788

Academic Editor: María Isabel Lamas Galdo

Received: 17 March 2023
Revised: 3 April 2023
Accepted: 4 April 2023
Published: 5 April 2023

Copyright: © 2023 by the authors. Licensee MDPI, Basel, Switzerland. This article is an open access article distributed under the terms and conditions of the Creative Commons Attribution (CC BY) license (https://creativecommons.org/licenses/by/4.0/).

1. Introduction

In recent years, rock-socketed concrete-filled steel tube piles (RSCFST) have been widely used in harbors, cross-sea bridges, offshore wind turbine pile foundation engineering, and other fields due to their excellent performance. Similar to concrete-filled steel tube piles (CFSTs), the confinement of the steel tube gives the concrete core a three-dimensional compression state, which effectively improves the compressive performance, plasticity, and toughness of the concrete core. The filling of the concrete core in turn prevents the premature local buckling of steel tubes and ensures the full implementation of steel materials [1–3]. In the construction process, steel pipes can also be used as templates to save time and reduce costs [4,5]. Different from CFSTs, only part of the steel tube is embedded in the bedrock in RSCFSTs, and thus there is a variation cross-section (VCS) in the rock-socketed section (Figure 1).

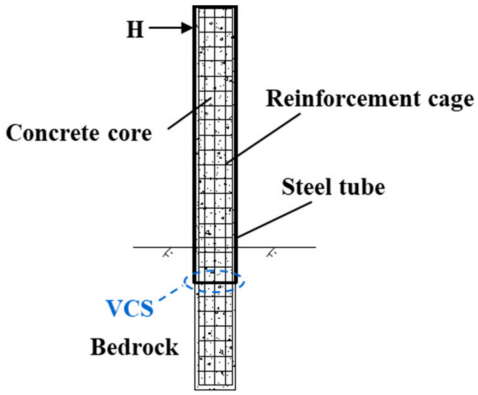


Figure 1. Illustration of the rock-socketed concrete-filled steel tube piles.

In practical engineering, the diameter of steel pipe in RSCFSTs exceeds 2 m, to enhance the bonding strength of the steel tube and concrete core interface (SCI) and realize the cooperative bearing of steel–concrete two-phase materials, so the structural type of longitudinal rebar is welded to the inner wall of the steel tube [6]. However, in the use stage of RSCFSTs, they are often subjected to horizontal loads that act in a low-cycle manner, such as impact force, the mooring force of a ship, wave force, and wind force [7–9]. RSCFSTs suffer fatigue damage under cyclic loading, and their cumulative plastic deformation increases, which eventually leads to the deterioration of long-term bearing performance. Therefore, it is necessary to study the horizontal bearing characteristics of RSCFSTs under horizontal cycle loading.

Previous studies mainly focused on the characteristics of CFSTs under axial and horizontal cyclic loading. Amit H. Varma et al. experimentally investigated the behavior of high-strength square concrete-filled steel tube beam-columns subjected to constant axial load and cyclically varying flexural load [10]. Yaochun Zhang et al. carried out horizontal cyclic loading tests on CFSTs considering axial force and cross-section shape, and the influence of axial force on the ultimate strength, stiffness, and ductility of steel tubular columns was analyzed [11]. Konstantinos. A et al. investigated the characteristics of CFSTs under constant compressive axial load and cyclic flexural load to analyze the seismic performance [1]. The effect of different sectional shapes and configurations on the eccentric axial load bearing capacity has also been investigated [12]. However, the characteristics of RSCFSTs under horizontal cyclic loading are rarely reported.

The interface bonding strength between the steel tube and concrete core is the key to ensuring the load transfer [13,14]. Previous studies have shown that the interface needs sufficient bonding strength to ensure the synergistic force between steel tube piles and core concrete [13–15]. A variety of connection forms to enhance interfacial bond strength have been proposed in the existing literature, such as shear studs [16–18], steel plates and steel bars [18], and internal rings [19]. Zhou studied the influence of casing constraints in rock-steel H-pile and the presence or absence of bolts in the H–steel–concrete interface on the bearing capacity through push-out experiments and pointed out that the bearing capacity of the H–steel–concrete column with bolts was the largest [20]. Zhang et al. showed that setting longitudinal reinforcement and filling concrete inside the steel plate can prevent local instability and improve the bearing capacity of the members [21]. The Robel Wondimu test showed that the bonding strength of the dense-spacing shear stud and the rib with a circular hole is the highest, followed by the rib and the wide-spacing shear stud [22]. Mingwei Liu et al. utilized the shear test to analyze the influence of the form of longitudinal rebar on the interfacial bonding strength and pointed out that the interfacial welding of longitudinal rebars can significantly improve the bonding strength [6]. The effectiveness of ordinary steel plates, saw-shaped steel plates, and perfobond leister steel plates in improving the bond strength at the steel tube–core concrete interface of CFST has also been investigated [23]. Peidai showed that adding internal rings can be an effective method for enhancing the bond strength of circular CFSST members [19].

At present, the existing literature focuses on push-out tests and push-out tests to explore the effects of welded ribs, circumferential reinforcement, and shear bond on the bonding strength of the SCI at the material level. However, few investigations have been conducted into the interfacial properties of RSCFSTs with welded longitudinal steel bars on the inner walls of the steel tubes under horizontal cyclic loads by using the large-scale physical model test.

In order to investigate the horizontal bearing characteristics of RSCFSTs under horizontal cyclic loading, this paper carried out cyclic loading tests under different horizontal loading conditions for RSCFSTs with a longitudinal rebar welded to the inner wall of the steel tube. The focus was mainly on the failure process of RSCFSTs, the development law of the lateral displacement-cycle loading times curve, and the cooperative bearing characteristics of the steel tube and the concrete core.

2. Experimental Procedure

2.1. Specimens Preparation

The RSCFST of the Chongqing Orchard Port wharf project was used as a prototype, and the test specimens were prepared according to the scale ratio of 1:7. A total of three identical RSCFST specimens were prepared for horizontal cyclic loading tests. The specimens were mainly composed of bedrock (foundation) and RSCFSTs (Figure 2a).

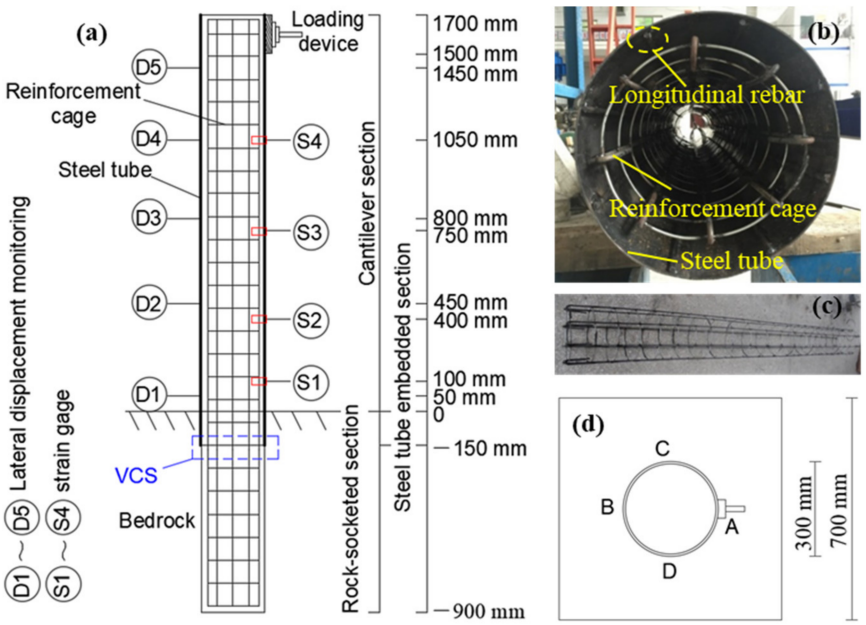


Figure 2. The preparation of specimens: (**a**) RSCFST specimen and the arrangement of monitor; (**b**) The steel tube, longitudinal rebar, and reinforcement cage of the RSCFST; (**c**) The reinforcement cage; (**d**) Top view of the specimen.

The foundation dimensions were 700 mm × 700 mm × 1500 mm, and it was placed in a coverless box composed of removable steel plates. The thickness of the steel plate was 100 mm, which had enough stiffness to limit the lateral deformation of the foundation.

The RSCFST was composed of a steel pipe, a longitudinal rebar, a reinforcement cage, and a concrete core (Figure 2a). The diameter D and thickness t of the steel tube were 300 mm and 2 mm, respectively. The total length of the steel tube was 1850 mm, with a cantilever section of 1700 mm and an embedded section of 150 mm (0.5D). Eight rebars with lengths of 1850 mm and diameters of 8 mm were welded longitudinally and equidistantly to the inner wall of the steel tube to enhance the bonding strength between the steel tube and the core concrete (Figure 2b). Eight rebars with lengths of 2800 mm and diameters of 8 mm were used to form the main steel bars of the reinforcement cage. According to

the Standard [24], both ends of the main steel bars were bent 100 mm, for anchorage. The stirrup was composed of 23 plain round bars with diameters of 4 mm. In the fabrication process of the stirrup, the lap length of 50 mm was welded to form a circular stirrup with a diameter of 252 mm. The stirrups were arranged equally along the main steel bars. The protective layer thicknesses of 20 mm and 10 mm were set along with the main steel bars and both ends of the reinforcement cage, respectively. The total length of the concrete core was 2600 mm, the cantilever length was 1700 mm, and the rock-socketed length was 900 mm (3*D*).

On side A of the cantilever section, strain gauges were arranged at four different height positions before pouring (Figure 2a,d), which were named S1~S4. Each position included three strain gauges, which were used to monitor the axial strain of the steel tube, the main steel bars of the reinforcement cage, and the concrete core, respectively, during the test. The strain gauge welded to the outer wall of the steel tube was used to measure the axial strain of the steel tube; the strain gauge welded to the main steel bars of the reinforcement cage was used to measure the axial strain of the main steel bars; the strain gauge attached to the precast concrete block fixed on the inner wall of the steel tube was used to monitor the strain of concrete core; and the distance between the strain gauge and the inner wall of the steel tube was 30 mm. A BE120-3BB-A (11) resistance strain gauge was adopted and a DH5922 dynamic signal strain acquisition system was used for acquiring strain data during the test. At the same time, five horizontal displacement monitoring points were arranged along the pile height on side B of the cantilever section (Figure 2a,d), which were named D1~D5. The type of displacement meter was WBD electromechanical percentile.

The process of producing the test piece began by pouring the foundation into the model box. Once the foundation reached the required strength, the water drill was used to drill the hole of the RSCFST. The processed steel tube and reinforcement cage were then placed and secured according to the designed position. Finally, C30 concrete was poured into the steel pipe to complete the specimen. The test was carried out after 28 days of curing.

2.2. Material Properties

Sandstone is the main bedrock of the coastal wharf in the upper reaches of the Yangtze River. Its compressive strength is 24.6 MPa and its saturated compressive strength is 18.9 MPa. In the test model, concrete pouring was used instead of bedrock. To better simulate the mechanical properties of sandstone, the final concrete mix ratio was determined by large trial tests. C15 concrete was selected for bedrock pouring, and the concrete core of the RSCFST was C30. The mixture ratio and mechanical properties are presented in Table 1.

Table 1. The mixture ratio and mechanical properties of concrete.

Concrete	Cement (kg/m^3)	Water (kg/m^3)	Fine Sand (kg/m^3)	Coarse Aggregate (kg/m^3)	7 Days Compressive Strength (MPa)	28 Days Compressive Strength (MPa)
C15	300.0	210.0	737.1	1152.9	11.39	15.14
C30	459.0	210.2	554.0	1176.8	26.28	38.70

The steel pipe was rolled and welded by a Q235-grade steel plate. The longitudinal rebar and the main steel bars of the reinforcement cage were ribbed bars, and the stirrup was a plain, round reinforcement. According to technical data provided by the manufacturer, the mechanical properties of the steel plate and steel bar are shown in Table 2.

Table 2. The properties of the steel material.

Position	Steel Size (t, d)	Yield Strength f_y (MPa)	Ultimate Strength f_u (MPa)	Elastic Modulus E_s (GPa)	Elongation δ (%)
Steel tube	2 mm	277.4	429.8	200	26
Stiffener bar main steel bar	8 mm	398.6	569.5	213	18
Hooping bar	4 mm	369.0	515.3	201	20

2.3. Loading Device and Loading Scheme

The test apparatus is a large port pile foundation test system that was developed jointly by Chongqing Jiaotong University and Hangzhou Bangwei Company. The system is mainly composed of a hydraulic source, a loading system (vertical and horizontal loading), a base, and a control and data acquisition system (Figure 3). The base is formed by reinforced concrete, and the reaction frame is composed of trusses. The bottom plate and the reaction frame have sufficient stiffness to ensure test accuracy. The surroundings and bottom of the specimen are fixed with high-strength bolts. The test loading system is based on the principle of the electro-hydraulic servo, with two loading modes of stress force control and displacement control, which can realize static tests, fatigue tests, and low-cycle repeated load tests.

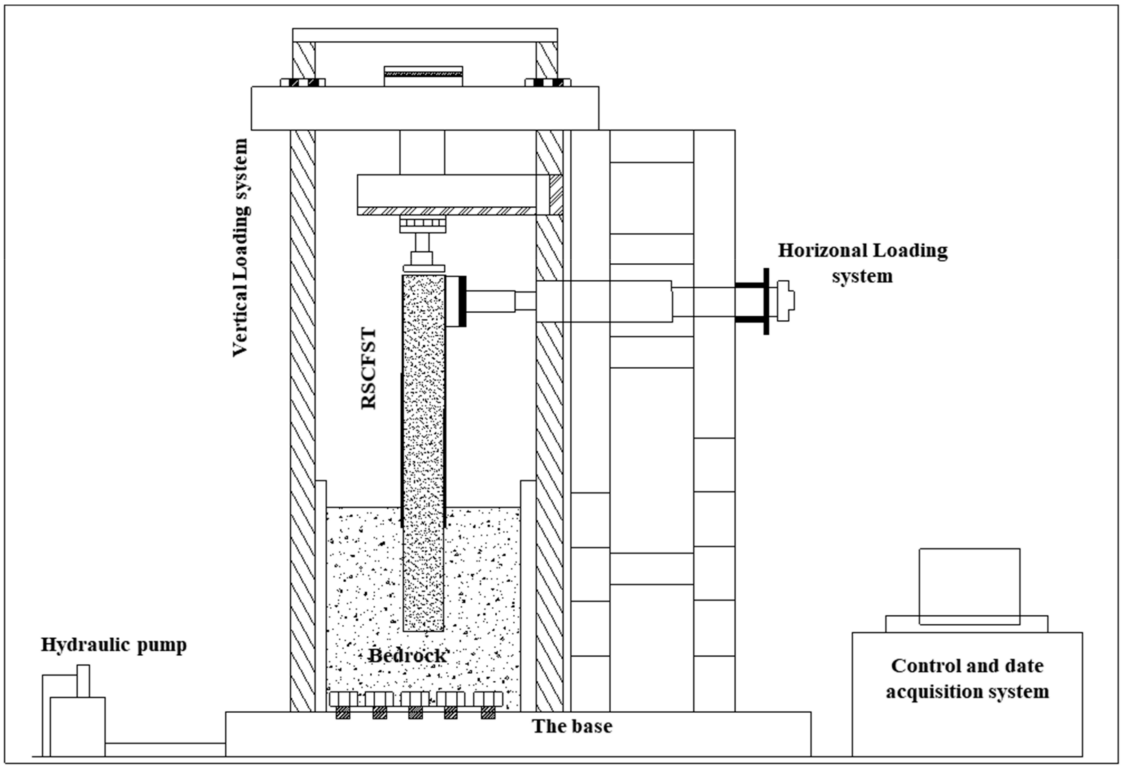


Figure 3. Test loading apparatus.

This study focuses on the influence of horizontal cyclic load on the bearing characteristic of the RSCFST, so the vertical load was not applied. A stress-controlled unidirectional horizontal cyclic loading method was adopted during the test. The loading frequency was set as 0.2 Hz after the repeated debugging of the test system. In practical engineering, the lateral force borne by RSCFST is mainly ship impact force, and the RSCFST was also subjected to the disturbance of water flow, wind, and waves. Through the finite element calculation, the threatening horizontal load H on a single pile of the wharf was found to be 9 kN under the normal impact force (with 1000 kN). Considering the factors of design

and the force majeure in the natural environment, the multiple relations of the threatening horizontal load on a single pile were adopted as the horizontal cyclic load during the test. The specimens were named SPA, SPB, and SPC, and the corresponding horizontal loads were 18 kN (2H), 22.5 kN (2.5H), and 27 kN (3H), respectively.

The pre-loading test was carried out before the start of the cyclic loading test, and the loading value of 0.2H was applied first to eliminate the adverse contact between the connectors and to test whether the test system was in a normal working state. Then, the cyclic loading test was carried out. The test was terminated when the foundation was obviously damaged or the displacement increased sharply.

3. Results and Discussion

3.1. Failure Characteristics

The experiment behaviors of the RSCFST specimens are discussed using the major events that occurred in the cyclic tests. These significant events are as follows:

A. The deboned steel tube in the rock-socketed part and the foundation interface (SFI) and the compacted foundation at sides A and B of the specimens (Figure 4a).
B. Concrete fracture at VCS (Figure 4b).
C. Cracks appear and spread at sides C and D of the foundation (Figure 4c).
D. The concrete core in the rock-socketed part was crushed and the SCI was deboned (Figure 4d).
E. Buckling of the steel tube in the rock-socketed part (Figure 4d).
F. Fatigue to fracture of the main steel bars at the VCS (Figure 4e).
G. Foundation destruction and RSCFST failure (Figures 4f and 5).

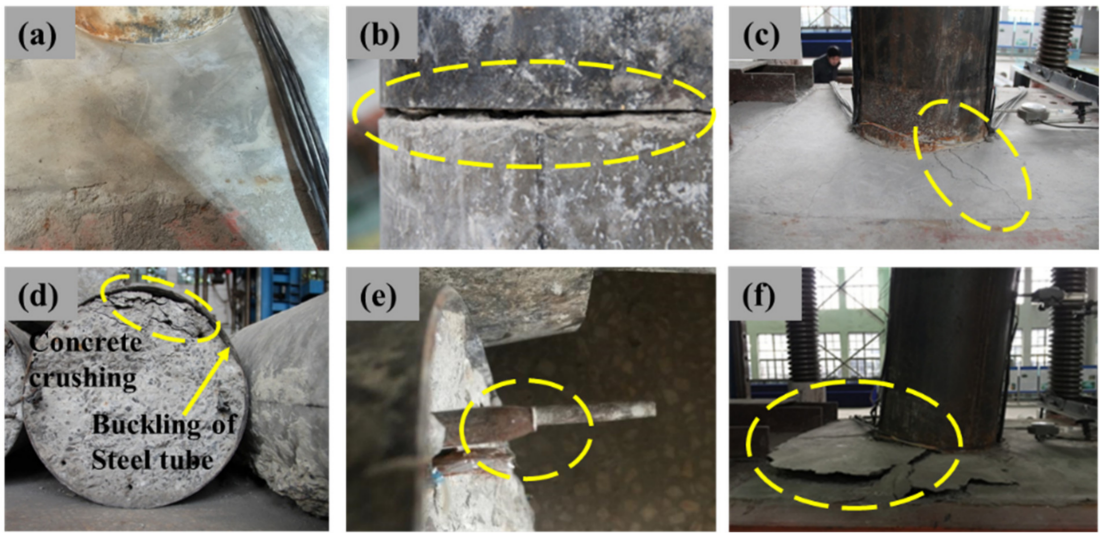


Figure 4. Failure characteristics of specimens: (**a**) Event A; (**b**) Event B; (**c**) Event C; (**d**) Event D and E; (**e**) Event F; (**f**) Event G.

Events A and B were obtained by combining the observation in the test, the dissection of the specimen after the test, and the force analysis. Event B means that the maximum bending moment point of the RSCFST moved down after the deboning of the SFI, and this further resulted in the cracking of the concrete core at the VCS. Events C, D, and F were obtained by observing the specimens after dissection and combining them with theoretical analysis; Event C means that the micro-cracks started to form and gradually expand at the sides C and D of the foundation under the tension stress caused by the horizontal load. The expansion direction of the micro-cracks was perpendicular to the loading direction of the horizontal load. At the same time, the micro-cracks also developed gradually to the depth of the foundation due to the repeated extrusion between the rock-socketed part of the RSCFST and the foundation. Event D represents the crushed concrete core and the deboned

SCI due to the repeated compression and shear between the rock-socketed part of the RSCFST and the foundation under cyclic loading. Event F is the transfer of the axial tensile force generated by the horizontal load to the main steel bars after the concrete cracked at the VCS. Then, the main steel bars were fatigued and this resulted in a necking fracture under repeated load application. Events E and G were obtained from direct observation during the test. Event E indicates that the embedded section of steel tube was deformed in flexure due to the crushing of the concrete core. Event G represents that the whole RSCFST was damaged.

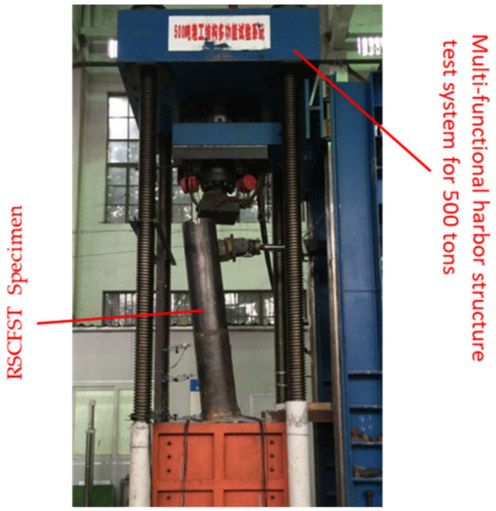


Figure 5. The failure of the RSCFST.

3.2. Lateral Deformation Characteristics of RSCFSTs under Horizontal Cyclic Loading

The lateral displacements of all specimens at different heights and the corresponding cyclic loading times were obtained by the data acquisition system. The total loading times n of specimens under the horizontal cyclic load can be used to characterize the working life of the RSCFST, and the n values of each test specimen are listed in Table 3. The n value of specimen SPA reached 68,000, while the n of SPB reduced significantly to 11,550, which is about 83% lower than that of SPA. The n of SPC is even worse and reduced to 7900, about 88% lower than that of specimen SPA. The results showed that when the horizontal cyclic load exceeds the unfavorable load, the horizontal bearing capacity of the RSCFST decreases nonlinearly with the increase in horizontal load.

Table 3. Test results.

Specimen	Number of Cycles						
	Total n	Stage I /n_1	n_1/n /%	Stage II /n_2	n_2/n /%	Stage III /n_3	n_3/n /%
SPA	68,000	10,500	15.44	50,500	74.26	7000	10.29
SPB	11,550	1920	16.62	8280	71.69	1350	11.69
SPC	7900	700	8.86	6700	84.81	500	6.33

Since the displacement meters of D3 and D4 failed during the test, we took the data at D1, D2, and D5 of each test specimen to draw the curves of lateral displacement—n (Figure 6). By comparing the lateral displacement curves of different specimens and the lateral displacement curves of the same specimen at different heights, it can be found that the lateral displacement development of the RSCFST under horizontal cyclic load presents the same trend. The lateral displacement—n curves are in an inverted "S" shape on the whole. From this curve, the development history of the lateral displacement can be divided

into three stages: (I) rapid growth period, (II) fatigue growth period, and (III) sharp growth period. These stages are distinguished by using magenta dotted line in Figure 6.

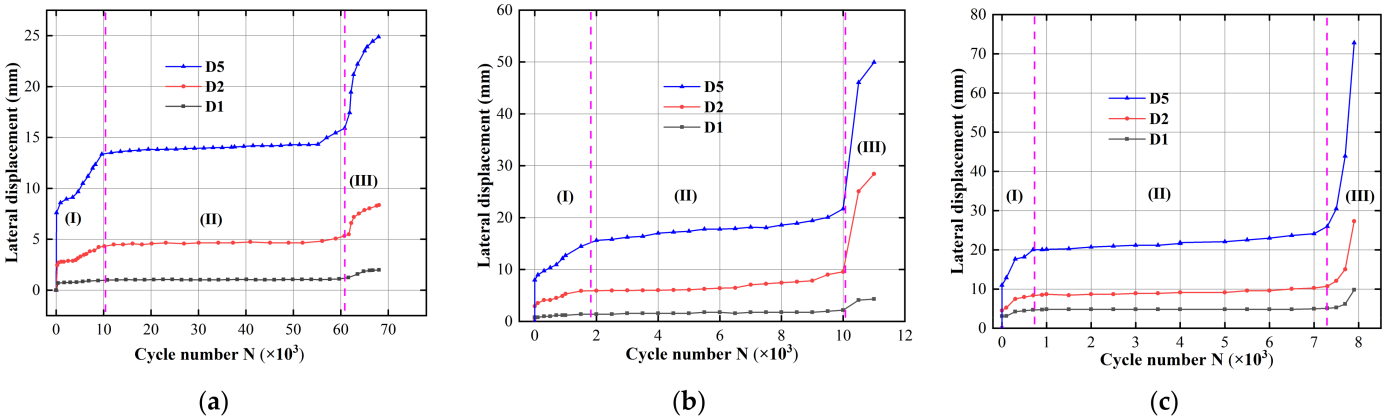


Figure 6. The curve of lateral displacement-cycle number: (**a**) SPA; (**b**) SPB; (**c**) SPC.

The number of loading cycle times n_i experienced by specimens in each stage is also listed in Table 2, and R = n_i/n is defined as the ratio of the loading times experienced by the specimens in each stage to the total loading times. During (I), the lateral displacements increased rapidly to a stable value within a short number of cycles. The R of specimens SPA, SPB, and SPC was 15.44%, 16.62%, and 8.86%, respectively, when the lateral displacements reached stability (Table 2). This shows that the larger the horizontal load is, the faster the lateral displacement reaches the stable value. Subsequently, within (II), the lateral displacement increased slowly with the increase in cyclic loading times, and this process lasted the longest time. The R of specimens SPA, SPB, and SPC was 74.26%, 71.69%, and 84.81%, respectively. In (III), the lateral displacement increased sharply, reflecting that the RSCFST specimen had failed. The R of process (III) for SPA, SPB, and SPC was 10.29%, 11.69%, and 6.33%, respectively. In addition, the lateral displacements at the same height in different specimens increased with the increase in the test load, which was in accordance with the theoretical force situation.

In conclusion, stages (I) and (II) can be regarded as the safe service period of the RSCFST, which accounts for about 90% of its total life. The safety service duration of SPA was the longest, while the safety service duration of SPB and SPC was about 16.72% and 10.49% of SPA, respectively.

The events in Section 3.1 can be utilized to explain the apparent segmentation of the lateral displacement-*n* curve. In (I), the events that occurred were mainly A and B. The SFI is mainly composed of chemical bonds that are so small they are almost negligible [7]. Thus, under horizontal loading, the SFI was firstly deboned and Event A occurred. Furthermore, this caused Event B to occur. Meanwhile, the foundation on the A and B side became compacted under the extrusion of the RSCFST. As a result, the deflection was deformed, the SFI was deboned, and the foundation compacting deformation produced by the RSCFST after loading caused the lateral displacement to rise rapidly during (I) and reach stability after the completion of events A and B. In (II), events C, D, E, and F appeared one after another under the repeated horizontal loads and formed a fatigue damage stage of relatively long duration. Since the stiffness of both the foundation and the RSCFST was large, the lateral displacement within this stage showed a slow growth trend with *n*. Stage (III) began with the occurrence of Event F. During (III), the RSCFST failed rapidly, and the surface of the foundation bulged under the thrust of the embedded rock section of the RSCFST, and eventually the structure as a whole was destroyed. Therefore, the lateral displacement in this stage increased sharply in a relatively short time.

3.3. Cooperative Bearing Characteristics of Steel Pipe and Core Concrete

The axial strain curves of the main steel bars, concrete core, and steel tube at different heights of each specimen with n are displayed in Figure 7. The axial strains of the main steel bars, concrete core, and steel tube vary significantly at different heights of the same specimen. The axial strains of the main steel bars, concrete core, and steel tube were the smallest at the S4 position, and the differences between the main steel bars and concrete core, concrete core and steel tube were also the smallest. It can be derived that the main steel bars, concrete core, and steel tube in the upper part of the RSCFST were in a very cooperative bearing state. This is because the upper part of the specimen is similar to a cantilever beam, and the bending moment under horizontal load is relatively small compared with the lower part. In this case, the bonding strength between the main steel bars and the concrete core and between the concrete core and the steel tube was sufficient to jointly withstand the relatively small strain generated by the bending moment. Additionally, the axial strain does not change significantly with the increase in n. In S3 and S2, the axial strains of the main steel bars, concrete core, and steel tube increase with the downward shift of the height, and the differences between the main steel bars and concrete core, and between the concrete core and the steel tube at the same location, also increase. This shows that the strain distribution on the main steel bars, concrete core, and steel tube changes as the section moves down. This is due to the increase in bending moment at the cross-section as it gets closer to the bottom. At the same time, the main steel bars and steel tube can withstand a greater bending moment because of their larger modulus of elasticity than the concrete core. Therefore, the strain on the main steel bars and steel tube is greater than that of the concrete core.

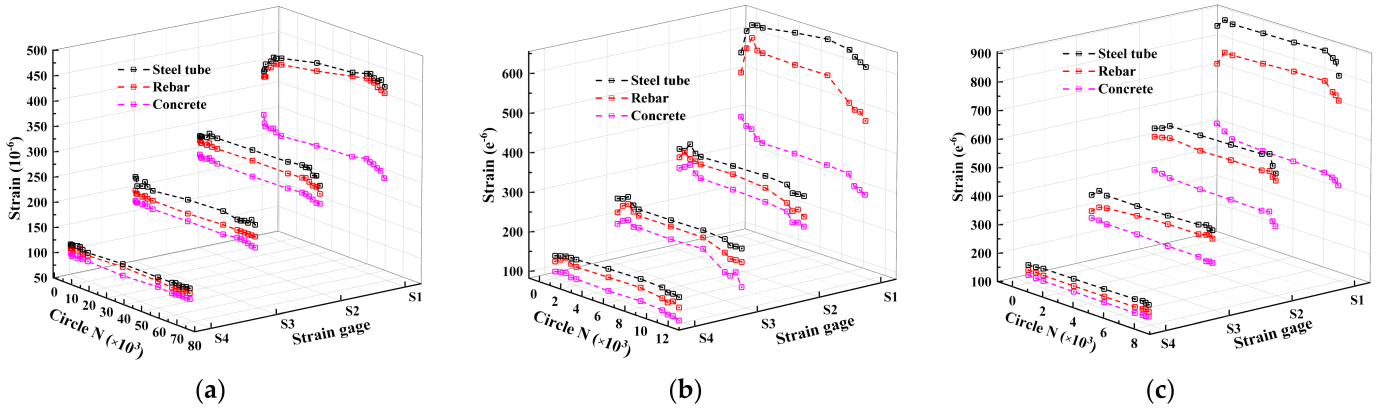


Figure 7. The axial strain curves of steel tube, the main steel bars and concrete core: (**a**) SPA; (**b**) SPB; (**c**) SPC.

During the whole test, the strain differences between the main steel bars and the concrete core, the concrete core and the steel tube at S4 and S3 of SPA, SPB, and SPC did not change significantly with the increase in n. This indicated that the bonding strength between the steel tube and the concrete core and between the concrete core and the main steel bars was in perfect condition and without relative slippage. Furthermore, the steel tube, the main steel bars, and the concrete core were still in a cooperative bearing state.

However, the strains on the main steel bars, the concrete core, and the steel tube all reach the maximum at the S1 position. At the initial stage, the bending moment at S1 was carried by the main steel bars, the concrete core, and the steel tube jointly. In (I), the strain generated in the concrete core decreased as n increased, while the strain in the main steel bars and the steel tube exhibited an increase with n. This is due to the occurrence of Event B, which caused a redistribution of the stress sharing among the main steel bars, the concrete core, and the steel tube in the cross-section at S1. During (II), the foundation cracks under the RSCFST extrusion, triggering Event D, which further led to the transfer of the bending moment at S1 and was mainly borne by the main steel bars and steel tube. As

a result, the strains of the main steel bars and steel tube gradually increase, and the strain of the concrete core continues to decrease, which also accelerates the fatigue damage of the main steel bars. Stage (III) began after the main steel bars began to fracture at the VCS. The strains of the main steel bars, steel tube, and concrete core all decreased in this stage, which marked the failure of the RSCFST.

In summary, it can be concluded that the SCI above S2 (about 7/10 of the length of the steel tube) remained bonded throughout the test, indicating that the longitudinal rebar welded to the inner wall of the steel tube provided sufficient bonding strength for the cooperative bearing between the steel tube and the concrete core. However, in the part lower than S2 (approximately 3/10 of the steel tube), deboning occurred at the SCI. The reason for this is that during the test, the concrete core at the lower part was crushed by compressive and shear action under the repeated extrusion between the RSCFST and bedrock. This mechanism was verified by cutting the RSCFST longitudinally and investigating the interface bonding state after the test (Figure 8a). Figure 8a shows the SCI in the rock-socketed section. The inner wall of the steel tube without the welded longitudinal rebar was deboned to form a smooth surface. At the inner wall, the welded rebar, the concrete core, longitudinal rebar and the inner wall of the steel tube are well combined. Under the test load, shear failure occurred at the concrete core. Figure 8b shows the SCI at the top of the RSCFST. The inner wall of the steel tube is still stuck with concrete, and the surface is rough, which indicates that the SCI is still well bonded and without relative slip.

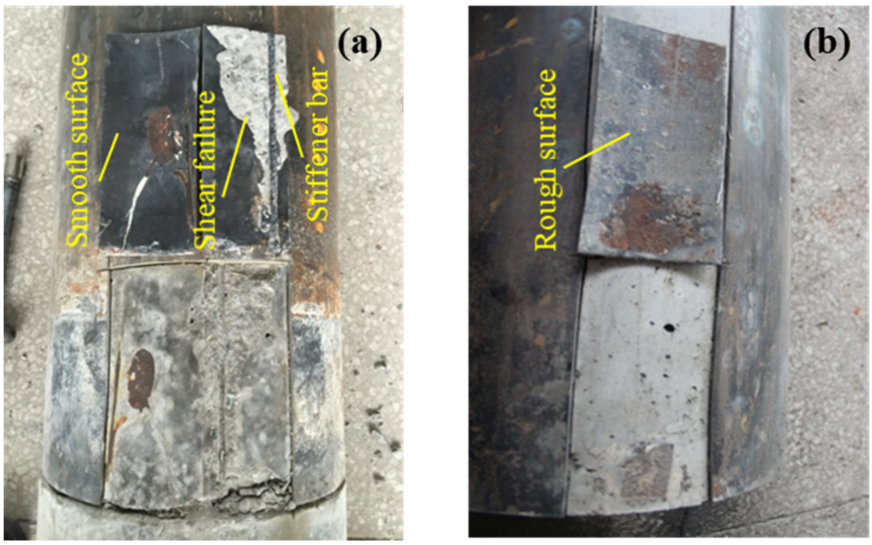


Figure 8. Bond state of steel and concrete interface: (**a**) The lower part of RSCFST; (**b**) The upper part of RSCFST.

3.4. Design Recommendations

From the above research, there are three main weaknesses in RSCFSTs. The first is the lack of foundation stiffness. Insufficient stiffness makes the foundation gradually crack after repeated loading and the maximum bending moment point of the RSCFST moves down, resulting in an increase in stress at the VCS and the main steel bars being subjected to fatigue damage and fracture. The second is the insufficient bonding strength between the steel tube and the concrete core interface at the lower part of the RSCFST. It is easy to lose interfacial bonding strength after loading when it is too small, which leads to the decrease in the cooperative bearing capacity of the two-phase material of steel tube and concrete and the deterioration of the performance of the structure. Third, the tension resistance ability at the VCS is insufficient, resulting in the fatigue fracture of the main steel bars. Given the above deficiencies, the following engineering measures are proposed:

Selection of a foundation of the RSCFST in bedrock with a greater stiffness.

Increasing the embedded depth of the steel tube to obtain higher foundation resistance.

Increasing the number of longitudinal rebars in the lower SCI of the RSCFST to enhance the bonding strength and improve the cooperative bearing capacity between the steel tube and the concrete core.

Increasing the number of main steel bars at the VCS or choosing ribbed steel bars with greater tensile strength to obtain greater fatigue resistance and improve the horizontal load bearing capacity of the RSCFST.

4. Conclusions

A horizontal cyclic load test of RSCFSTs was carried out, and the variation law of the lateral displacement with the cyclic loading times and the failure process of RSCFSTs were discussed. The cooperative bearing characteristics of the interface between the steel tube and the concrete core were analyzed throughout the test. Within the scope of this study, the following conclusions can be drawn:

(1) The horizontal bearing capacity of RSCFSTs decreases nonlinearly with the increase in horizontal load. Under horizontal cyclic loading, the lateral displacement of the RSCFST experienced: (I) rapid growth period, (II) fatigue growth period, and (III) sharp growth period. The duration of the rapid growth period and fatigue damage period accounted for about 90% of the total life of the RSCFST.

(2) The stiffening form of the welded longitudinal rebar makes the SCI of the upper part of the RSCFST have sufficient bonding strength to bear the horizontal load jointly. However, in the lower part of the RSCFST, the interface between the steel tube and concrete core was deboned due to compression-shear failure, resulting in poor cooperative bearing performance between the steel tube and concrete core.

(3) Insufficient foundation stiffness, SCI bonding strength, and fatigue strength at the VCS are the shortcomings in RSCFSTs. Our recommended suggestions regarding practical engineering include selecting bedrock with better stiffness as the foundation, increasing the embedded depth of the steel tube, adding a sniffer bar between the SCI, and enhancing the main reinforcement at the VCS, to improve the horizontal bearing capacity of RSCFSTs.

Through the research presented in this paper, several qualitative and useful conclusions have been obtained. However, it should be noted that the model test of RSCFSTs without stiffening the steel tube has not yet been carried out for comparison, and finite element analysis needs to be further investigated. Additionally, structural optimization needs to be researched in a future study as well. In our follow-up work, we will focus on these important issues in order to promote the development of theoretical research on RSCFST structure, as this would be of important scientific value and provide useful guidance for practical engineering applications.

Author Contributions: Investigation, conceptualization, methodology, M.L.; formal analysis, writing—original draft preparation, F.W.; supervision, resources, E.A.; validation, L.W.; data curation, visualization, Y.H.; visualization, N.C.; data curation, visualization, J.C. All authors have read and agreed to the published version of the manuscript.

Funding: This research was funded by supported by the National Natural Science Foundation of China (No.52279124, 41907261) and The Talents Plan Project in Chongqing of China (cstc2021ycjh-bgzxm0053, cstc2021 yszx-jcyjX0002).

Institutional Review Board Statement: Not applicable.

Informed Consent Statement: Not applicable.

Data Availability Statement: Not applicable.

Conflicts of Interest: The authors declare no conflict of interest.

References

1. Skalomenos, K.A.; Hayashi, K.; Nishi, R.; Inamasu, H.; Nakashima, M. Experimental Behavior of Concrete-Filled Steel Tube Columns Using Ultrahigh-Strength Steel. *J. Struct. Eng.* **2016**, *142*, 04016057. [CrossRef]
2. Ho, J.C.M.; Ou, X.L.; Li, C.W.; Song, W.; Wang, Q.; Lai, M.H. Uni-axial behaviour of expansive CFST and DSCFST stub columns. *Eng. Struct.* **2021**, *237*, 112193. [CrossRef]
3. Szadkowska, M.; Szmigiera, E. Analysis of shrinkage influence on bond in CFST elements filled with SCC. *J. Constr. Steel. Res.* **2021**, *184*, 106824. [CrossRef]
4. Lehman, D.; Roeder, C.; Heid, A.; Maki, T. Shear response of concrete filled tubes part 1: Experiments. *J. Constr. Steel. Res.* **2018**, *150*, 528–540. [CrossRef]
5. Zhang, Y.T.; Shan, B.; Xiao, Y. Axial impact behaviors of stub concrete-filled square steel tubes. *Adv. Struct. Eng.* **2019**, *22*, 2490–2503. [CrossRef]
6. Liu, M.W.; Wu, F.Y.; Abi, E.D.; Wu, L.J.; Su, G.Q. Strength Degradation Characteristics of the Steel-Concrete Interface Under Cyclic Shear. *Teh. Vjesn.* **2022**, *29*, 1372–1381. [CrossRef]
7. He, R.; Ji, J.; Zhang, J.; Peng, W.; Sun, Z.; Guo, Z. Dynamic Impedances of Offshore Rock-Socketed Monopiles. *J. Mar. Sci. Eng.* **2019**, *7*, 134. [CrossRef]
8. Liu, J.; Guo, Z.; Zhu, N.; Zhao, H.; Garg, A.; Xu, L.; Liu, T.; Fu, C. Dynamic Response of Offshore Open-Ended Pile under Lateral Cyclic Loadings. *J. Mar. Sci. Eng.* **2019**, *7*, 128. [CrossRef]
9. Jenck, O.; Obaei, A.; Emeriault, F.; Dano, C. Effect of Horizontal Multidirectional Cyclic Loading on Piles in Sand: A Numerical Analysis. *J. Mar. Sci. Eng.* **2021**, *9*, 235. [CrossRef]
10. Amit, H.V.; James, M.R.; Richard, S.; Lu, L.W. Seismic Behavior and Design of High-Strength Square Concrete-Filled Steel Tube Beam Columns. *J. Struct. Eng.* **2004**, *130*, 169–179. [CrossRef]
11. Zhang, Y.; Xu, C.; Lu, X. Experimental study of hysteretic behaviour for concrete-filled square thin-walled steel tubular columns. *J. Constr. Steel. Res.* **2007**, *63*, 317–325. [CrossRef]
12. Kim, C.S.; Park, H.G.; Chung, K.S.; Choi, I.R. Eccentric Axial Load Capacity of High-Strength Steel-Concrete Composite Columns of Various Sectional Shapes. *J. Struct. Eng.* **2014**, *140*, 04013091. [CrossRef]
13. Xue, J.Q.; Briseghella, B.; Chen, B.C. Effects of debonding on circular CFST stub columns. *J. Constr. Steel. Res.* **2012**, *69*, 64–76. [CrossRef]
14. Wang, X.L.; Fan, F.F.; Lai, J.X. Strength behavior of circular concrete-filled steel tube stub columns under axial compression: A review. *Constr. Build. Mater.* **2022**, *322*, 126144. [CrossRef]
15. Roeder, C.W.; Cameron, B.; Brown, C.B. Composite Action in Concrete Filled Tubes. *J. Struct. Eng.* **1999**, *125*, 477–484. [CrossRef]
16. Dong, H.Y.; Chen, X.P.; Cao, W.L.; Zhao, Y.Z. Bond-slip behavior of large high-strength concrete-filled circular steel tubes with different constructions. *J. Constr. Steel. Res.* **2020**, *167*, 105951. [CrossRef]
17. Dong, H.Y.; Chen, X.P.; Cao, W.L.; Zhao, Y.Z. Bond behavior of high-strength recycled aggregate concrete-filled large square steel tubes with different connectors. *Eng. Struct.* **2020**, *211*, 110392. [CrossRef]
18. Qiao, Q.Y.; Zhang, W.W.; Qian, Z.W.; Liu, W.C. Experimental Study on Mechanical Behavior of Shear Connectors of Square Concrete Filled Steel Tube. *Appl. Sci.* **2017**, *7*, 818. [CrossRef]
19. Peng, D.; Yang, L.; Wang, J.; Fan, J.W.; Lin, M.F. Experimental study on the steel–concrete bond behaviour of circular concrete-filled stainless steel tubes. *Thin-Walled Struct.* **2021**, *9*, 108506. [CrossRef]
20. Zhou, Y.D.; Tham, L.G.; Tang, X.W.; Liu, Y.T.; Wong, M.K. Parametric analyses of push-out tests and implications for design of rock-socketed steel H-pile. *Comput. Geotech.* **2011**, *38*, 383–392. [CrossRef]
21. Zhang, J.G.; Liu, Y.J.; Yang, J.; Xu, K.L. Experimental Research and Finite Element Analysis of Concrete-Filled Steel Box Columns with Longitudinal Stiffeners. *Adv. Mater. Res.* **2011**, *287–290*, 1037–1042. [CrossRef]
22. Alemayehu, R.W.; Bae, J.; Ju, Y.K.; Park, M.J. Bond Behavior of Concrete-Filled Steel Tube Mega Columns with Different Connectors. *Materials* **2022**, *15*, 2791. [CrossRef] [PubMed]
23. Peng, D.; Yang, L.; Wang, J.; Lin, M.F.; Fan, J.W. Bond stress-slip relationship in concrete-filled square stainless steel tubes. *Constr. Build. Mater.* **2022**, *326*, 127001. [CrossRef]
24. *JTS 144-1-2010*; Load Code for Harbour Engineering, Ministry of Transport of the People's Republic of China. China Communications Press: Beijing, China, 2010.

Disclaimer/Publisher's Note: The statements, opinions and data contained in all publications are solely those of the individual author(s) and contributor(s) and not of MDPI and/or the editor(s). MDPI and/or the editor(s) disclaim responsibility for any injury to people or property resulting from any ideas, methods, instructions or products referred to in the content.